

# A universal all-dry microfabrication method for sensitive electronic materials via an inorganic molecular lithographic mediator

---

Received: 31 July 2025

---

Accepted: 12 January 2026

---

Cite this article as: Zeng, C., Xu, Y., Wei, X. *et al.* A universal all-dry microfabrication method for sensitive electronic materials via an inorganic molecular lithographic mediator. *Nat Commun* (2026). <https://doi.org/10.1038/s41467-026-68593-z>

Cheng Zeng, Yongshan Xu, Xinqi Wei, Jianing Liang, Zongdong Sun, Xiaoyu He, Gaofeng Du, Shuhao Wang, Yao Liu, Xing Zhou, Yuan Li, Kailang Liu, Ying Ma, Tianyou Zhai & Huiqiao Li

---

We are providing an unedited version of this manuscript to give early access to its findings. Before final publication, the manuscript will undergo further editing. Please note there may be errors present which affect the content, and all legal disclaimers apply.

If this paper is publishing under a Transparent Peer Review model then Peer Review reports will publish with the final article.

---

**A universal all-dry microfabrication method for sensitive electronic materials via an  
inorganic molecular lithographic mediator**

Cheng Zeng<sup>1,2</sup>, Yongshan Xu<sup>2</sup>, Xinqi Wei<sup>2</sup>, Jianing Liang<sup>2,3</sup>, Zongdong Sun<sup>2</sup>, Xiaoyu He<sup>2</sup>, Gaofeng Du<sup>2</sup>,  
Shuhao Wang<sup>1</sup>, Yao Liu<sup>2</sup>, Xing Zhou<sup>2</sup>, Yuan Li<sup>2</sup>, Kailang Liu<sup>2</sup>, Ying Ma<sup>2</sup>, Tianyou Zhai<sup>2</sup>✉, Huiqiao Li<sup>1,2</sup>✉

<sup>1</sup>Key Laboratory of Flexible Optoelectronic Materials and Technology (Ministry of Education), School of Optoelectronic Materials & Technology, Jianghan University, Wuhan, China. <sup>2</sup>State Key Laboratory of Materials Processing and Die and Mould Technology, School of Materials Science and Engineering, Huazhong University of Science and Technology, Wuhan, China.

<sup>3</sup>Hubei Yangtze Memory Laboratories, Wuhan, China

✉ e-mail: hqli@hust.edu.cn; zhaity@hust.edu.cn

## Abstract

Lithography is pivotal in fabricating micro/nanoscale patterns and processing materials for electronic microdevices. However, conventional organic polymeric resists inevitably entail the use of various chemical solutions or solvents, which especially compromise fragile electronic materials featuring atomic-level surfaces. Here, we introduce inorganic selenium molecules as a lithographic mediator for sensitive electronic material processing without direct exposure to solutions or solvents. Specifically, the inorganic selenium molecular film functions as both a lithographic mediator for direct patterning due to its weak intermolecular van der Waals interactions, and as a protective encapsulation layer for atomic electronic materials without compromising structural and electronic characteristics. Wafer-scale arrays of sensitive materials with high-quality sharp edges are facilely achieved by a non-destructive mechanical peeling of the

---

selenium layer. This approach provides a solvent-free lithographic route for microfabricating sensitive materials and high-performance electronic devices.

ARTICLE IN PRESS

## Introduction

Lithography underpins modern semiconductor manufacturing <sup>1,2</sup>, widely used in electronic systems<sup>3</sup>, integrated circuits<sup>4,5</sup>, and flexible electronic devices<sup>6,7</sup>, which allows micro/nanopatterning through a series of physical-chemical reactions between photons or electrons interacting with sensitive resist<sup>8-13</sup>. The commercial organic resist is a critical-formulated polymer composite of phenolic resin, photosensitizer, solvent<sup>14</sup>. The processes based on the conventional organic resists use kinds of solutions and solvents, including developer, remover, and cleaner. Such solutions or solvent residuals are inevitably adsorbed on the sample's surface or substrate, potentially scattering the local concentration of charge carriers and disrupting charge transportation<sup>15-17</sup>, especially in modern two-dimensional electronic devices and atomic-scale monolayer materials with large specific surface areas. In addition, for high-sensitive electronic materials such as perovskite, black phosphorus (BP), and halides<sup>18-21</sup>, such solutions or solvents can even induce chemical reactions or doping, critically degrading the structural integrity of the functional materials<sup>22,23</sup>. For example, phosphorus atoms are prone to irreversible oxidation while black phosphorus contacts with solvents due to the easy transfer of the lone pair electrons<sup>24</sup>. Applying a chemically stable protective layer (such as graphene or boron nitride) over the surface of sensitive materials allows for minimized corrosion and contamination from solvents<sup>25,26</sup>. Unfortunately, the approaches introduce added complexity to the device construction and make it challenging to be compatible with the staple semiconductor industry integration processes. The conventional organic resist does not accommodate microfabrication of solvent-sensitive electronic

---

materials with considerable potential.

Here we explore the inorganic selenium molecules as a microlithographic mediator for sensitive electronic materials. Selenium molecules directly pattern with a localized photothermal sublimation sequentially under irradiation, due to weak van der Waals forces between the molecule units. In addition, adhesion discrepancy between the selenium layer and substrate is introduced to easily mechanically peel the selenium film at wafer scale for object patterns, ensuring a high-clean contact interface. Based on the inorganic molecular processing, a non-destructive micropatterning for high-sensitive materials, halides, and perovskites, was successfully realized. The process is compatible with large-area array device preparation of sensitive electronic materials, and the prepared field effect transistors exhibit a high electronic transport. In addition, the inorganic selenium molecular medium is simple in composition, controllable in thickness, and inexpensive compared to conventional organic photoresists. The inorganic molecular strategy realizes the solvent-free micropatterning of solvent-sensitive electronic materials, which is vital for the large-scale integration of novel two-dimensional electronic materials and high-performance microelectronic devices.

## Results

### **Inorganic selenium molecular microlithographic mediator**

Conventional micro/nanofabrication processes based on inorganic polymer mediator routinely employ chemical reagents such as photoresists, developing agents, and cleaning solutions, which

inherently contain organic solvents, aqueous components, and even corrosive alkaline solutions. Upon interfacial contact between these chemical agents and sensitive materials, they readily induce interfacial damage, including dissolution of functional constituents, surface defect, and contaminant residue, especially to sensitive materials (Fig. 1a). Elementary selenium, known as an inorganic molecular material, is used as the lithographic mediator for the protective processing of sensitive materials in this work. A uniform wafer-scale film can be easily obtained by simple thermal vapor deposition from commercial selenium powder at a low temperature (150 °C) (Fig. 1b, Supplementary Fig. 1). The deposited selenium films exhibit close contact with the substrate, a dense and smooth surface, and a uniform and adjustable thickness (Fig. 1c, Supplementary Fig. 2-4). Essentially, the amorphous selenium film was constructed by isolated selenium species such as small molecular rings and chain fragments linked by weak van der Waals interaction (Supplementary Fig. 5)<sup>27-29</sup>. When exposed to irradiation, the weak intermolecular van der Waals interactions are easily broken up by the absorbed outside energy<sup>30</sup>. Thus, the irradiated partial region of the selenium film would be exposed by the localized thermal sublimation of small molecular fragments, forming a designed pattern (Fig. 1d). This robust stability significantly bolsters the case for the applicability in real manufacturing environments. A series of consecutive Raman spectra were collected to monitor selenium molecular structure during laser irradiation (Supplementary Fig. 6). Specifically, the irradiated point on the selenium surface immediately hole formation as selenium molecular volatilization and exposed the substrate under the sensitive wavelength laser irradiation. Micropatterns with different shapes and feature sizes are directly

obtained by laser writing in the selenium film, with no need of the development step in conventional lithography. Straight line patterns can be easily achieved for micro-scale features with 1  $\mu\text{m}$  trenches and 2  $\mu\text{m}$  lines (Fig. 1e, Supplementary Fig. 7). The statistics of trenches and lines show that the patterns are of high quality in width uniformity. With different thicknesses, selenium films are still patterned with clear boundaries (Supplementary Fig. 8). The resolution of the line micropatterns can be adjusted and optimized by laser beam parameters, such as output powers, Laser wavelength, and scanning speeds (Supplementary Fig. 9-11). For instance, the 532 nm laser produces a finer resolution of approximately 1.1  $\mu\text{m}$  than the 633 nm. This is attributed to the higher photon energy and potentially tighter focal spot achievable with the shorter wavelength, leading to more confined photothermal energy and thus finer feature definition. As for the etched trench precision, three-dimensional AFM topographic images suggest that the patterns obtained are sharp edges in the unexposed area (Supplementary Fig. 11). The irradiated areas exhibit similarly minimal height variations (-0.3 nm~0.4 nm) and nearly identical image roughness values (Ra: 0.42 nm~0.45 nm), which indicate the presence of discrete nanoparticles and support a residue-free patterning process (Supplementary Fig. 12). Large area XPS detections consistently find no Se characteristic signs in the substrate, suggesting that the proposed method enables the complete removal of selenium molecules (Supplementary Fig. 13). Additionally, complementary distributions of Se and substrate (Si) signal strength in elemental mapping demonstrate that selenium molecules in the unexposed area are not affected during laser irradiation (Supplementary Fig. 14). Precisely spatial control of laser beam movement enables to obtain

various delicate micropatterns, such as array patterns, line patterns, curvilinear patterns, character patterns, and numeric patterns (Supplementary Fig. 15). Complex patterns with various sharp angles and curves can also be obtained by direct writing (Fig. 1f). The direct lithography excludes contamination with chemical organic solvent or solution, showing more simple processing for structures and materials.

### **Inorganic molecular mediator towards sensitive materials**

The inorganic selenium molecular microlithography is particularly suited to processing sensitive materials. The direct sublimation lithographic etching and drying removal processes avoid solvent-induced damage, preserving the structural and electronic characteristics of the functional materials. As proof of the feasibility, we chose different kinds of representative sensitive materials to compare the inorganic selenium lithography with standard organic polymer lithography (Fig. 2a,b). Typical solvent-sensitive samples, such as halide  $[\text{PbBr}_2]$ , perovskite  $[(\text{MP})_2\text{PbI}_4]$ , and alkali metal compound  $[\text{LiInP}_2\text{S}_6]$ , phosphorus sulfide  $[\text{MgPS}_3]$ , black phosphorus  $[\text{BP}]$  (Fig. 2c-g, Supplementary Fig. 16), are covered with selenium molecular layer and organic polymer photoresist layer, respectively. In the exposed windows, these sensitive materials can maintain the original morphology through selenium microlithography (Fig. 2h-2l). Furthermore, these solvents can induce chemical reactions or doping, degrading the structural integrity of the functional materials, especially for halide  $[\text{PbBr}_2]$  and perovskite  $[(\text{MP})_2\text{PbI}_4]$  (Fig. 2m-2q). The organic polymer resist induces structural defects and damage to BP atomic surface, and residues in the substrate, which would cause charge carrier scattering (Fig. 2q, Supplementary Fig. 17). The

disappearance or shift of Photoluminescence (PL) and Raman signals indicates that the crystal structures have been seriously damaged during the organic resist lithography process (Fig. 2r-2t). Whereas, the detected optical signs remain completely consistent during the selenium lithography process, demonstrating that the non-destructive superiority of the inorganic selenium process is more pronounced in the non-destructive processing of solvent-sensitive materials (Fig. 2r-2t, Supplementary Fig. 18,19).

### **Wafer-scale micropatterns by physical lift-off process**

Thin-film deposition and patterning are the fundamental steps to integrate any novel material into a miniaturized device. The proposed inorganic molecular microlithography involves coating an inorganic molecular lithographic mediator layer on substrate, laser/plasma exposure to patterning, object material preparation, and removing a lithographic mediator (Fig. 3a). In conventional organic lithography, solvents such as acetone and ethanol are used to remove residual photoresist during the lift-off process, potentially damaging the functional objective samples especially for those sensitive to solvents. To avoid this issue, we develop an effective physical approach for drying removal of the selenium mediator layer by virtue of polydimethylsiloxane (PDMS) adhesion (Fig. 3b). Specially, PDMS, as an elastomer with low modulus and low surface energy, easily establishes a closely conformal contact with object sample lamination, via van der Waals interaction adhesion<sup>31,32</sup>. Qualitatively comparison by mechanically separating the layers in different stacking orders found that the adhesion at different contact interfaces between adjacent

layers possesses radical discrepancy (Supplementary Fig. 20). Among them, the interfacial adhesion between the selenium film and the substrate (F2) is much weaker than that of the object layer and substrate (F1), which is the key to enabling the successful physical removal of the selenium mediator layer (Supplementary Fig. 21, Supplementary Movie 1). Nano-scratching measurement was used to further quantitative test the adhesive force between the different contact interface (Supplementary Fig. 22). Consequently, the average adhesive force represented as critical load parameter is 1.35 mN for the selenium/substrate interface (F2), lower than that of the object/substrate

(F1, 7.34 mN) (Fig. 3c, Supplementary Fig. 23). The weak interfacial adhesion allows to easily remove the redundant selenium mediator by physically peeling off from the substrate, without the assistance for any chemical solutions.

To verify the peeling function above, we fabricate the different object micropatterns by the inorganic selenium lithography (Fig. 3d). Before the object patterning, large-area redundant Se/object layer can be completely separated from substrate (Fig. 3e). For example, metal Au pattern and arrays can be easily fabricated by the drying lift-off process (Supplementary Fig. 24-26). The van der Waals interactions of PDMS with the object layer are the crucial characteristics during lift-off process (Supplementary Fig. 27). Except for the interfacial contact, the boundary contact between the selenium molecular layer and the metal layer is another critical factor in determining the final quantity of the patterns. Object patterns with straight boundary and curved boundary were investigated, respectively. After PDMS removal, the resulting edge of metal layer

is completely complementary to the straight edge of the original selenium film (Supplementary Fig. 28a). The complementarity is highly matching even in extremely curved boundary (Supplementary Fig. 28b). The proposed microlithography approach based on interfacial adhesion discrepancy enables to preparation of high-quality metal electrode patterns.

Further, large-area sensitive material arrays are also prepared by this mechanical peeling method, as exemplified by electronic halide lead bromide ( $PbBr_2$ ) materials (Fig. 3f, Supplementary Fig. 29, Supplementary Movie 2). Different density arrays can be presented simultaneously after one-step mechanical peeling. Wafer surface cleanliness after processing is a vital index sign in evaluating lift-off effect. AFM topographic image of  $SiO_2/Si$  substrate after lift-off process shows that the surface undulation is consistent with the fresh silicon surface in the range from  $-1\text{ nm}$  to  $1\text{ nm}$  (Fig. 3g). It indicates that the silicon surface is

quite clean with no remnant selenium particles or metal particles after the physical peeling processes. In contrast, organic polymer mediator leave a large amount of residues on the substrate, which will directly affect the performance of electronic materials (Supplementary Fig. 30). In a word, the selenium microlithographic process can achieve a high cleanliness with the auxiliary PDMS. It is worth noting that one physical peeling step can simultaneously achieve different array patterns of varying densities in one wafer. Fig. 3h shows six pattern arrays obtained in the same wafer after lift-off by peeling. All of the small 30 patterns random chosen from array I to array VI show uniform size and height (Supplementary Fig. 31). Statistical half violins of pattern roughness (average  $0.85\text{ nm}$ ), pattern-substrate vertical angle (average  $92^\circ$ , containing probe moving error in

step), and substrate roughness (average 0.35 nm) demonstrate the flat pattern surface, sharp edge, and clear substrate (Fig. 3i). The wafer-scale fabrication of the high-quality halide lead iodide  $\text{PbI}_2$  pattern arrays strongly confirms the solid accessibility and reliability of the selenium molecular microlithography for sensitive materials (Supplementary Fig. 32). Importantly, the simplified selenium microlithography does not involve any chemical solvent or solution contact to sensitive materials, comparison with the standard organic resist lithography (Supplementary Fig. 33, Supplementary Movie 3). In addition, compared with other dry fabrication strategies, including shadow mask techniques and mechanical transfer methods, the organic selenium-mediated method uniquely combines: high resolution and freedom pattern design on a single substrate without custom masks, and less surface contamination without transfer polymers. This low-contamination and non-destructive method provides a reliable foundation for the preparation of high-performance electronic devices.

### **Microlithography for 2D material electronic device**

To verify the applications of such the drying microlithography process in electronic device fabrication, we further fabricate two-dimensional material field-effect transistors (FET) by selenium molecular lithographic technology (Figure 4a). The channel material used is the typical sensitive BP and monolayer  $\text{MoS}_2$ . BP is highly sensitive to solvent, surface absorption, and contamination, which usually needs extra special protection measurements when served in electronic devices<sup>24,33,34</sup>. The exfoliated BP flake on the substrate is

contacted with metal Au as drain and source electrodes, and the doped Si covered by SiO<sub>2</sub> layer (300 nm) is used as the back gate and gate dielectric. During our fabrication process, the surface atoms of the BP layer are covered by the selenium molecular mediator, which avoids contact erosion toward BP from solution/solvent/air. Figure 4b illustrates the optical microscopy images of a single BP FET device before and after metal electrode construction. The transfer characteristics ( $I_{ds}$ - $V_{gs}$ ) of the transistor show a typical P-type behavior (Fig. 4c). The achieved on/off ratio is competitive with, and in some cases superior to, that of reported for BP devices (Supplementary Fig. 34 and Supplementary Table 1). The linear output curves ( $I_{ds}$ - $V_{ds}$ ) in Fig. 4d suggest nearly ideal ohmic contact behavior. The inorganic selenium molecular mediator allows a high-cleanness surface for efficient carrier transport.

The inorganic selenium molecules integrated microlithography enables the large-area microelectronic fabrication of field-effect transistor arrays (Supplementary Fig. 35). Fig. 4e shows the fabricated FETs based on monolayer molybdenum disulfide (MoS<sub>2</sub>) device with a channel length ( $L_{ch}$ ) of 25  $\mu$ m and channel width ( $W_{ch}$ ) of 10  $\mu$ m. MoS<sub>2</sub> is considered to be a potential channel electronic material due to its adjustable band gap and high mobility<sup>35-37</sup>. The  $I_{ds}$ - $V_{ds}$  transfer curves with drain-source voltage at 0.5 V show typical n-type transistor characteristics. Histogram statistical analyses in Fig. 4f confirm the spatially uniform n-type transistor operation with reliable electrical performance in parameters on-current  $I_{on}$  and on-off ratio with Gaussian distribution. The average and best on-off ratios are about 10<sup>7</sup> and 10<sup>9</sup>, respectively. For comparison, two MoS<sub>2</sub> FET arrays with the same channel length and width ( $L_{ch}/W_{ch}=12/5$   $\mu$ m) are fabricated

by inorganic selenium molecular lithography and traditional organic resist lithography, respectively (Supplementary Fig. 36). The FET devices by the inorganic microlithography exhibits a higher on/off ratio ( $10^8$ - $10^9$ ) and much improved electronic uniformity than that of organic resist (Fig. 4g), suggesting the atomic structure of sensitive materials can be greatly maintained during the selenium microlithographic fabrication. The devices achieve an average on/off ratio that is significantly higher than those of other reported back-gated MoS<sub>2</sub> FETs with SiO<sub>2</sub> dielectric fabricated by the organic resist lithography, by over an order of magnitude against most references and about fivefold against the highest benchmark<sup>17,37-48</sup> (Fig. 4h and Supplementary Table 2). Electronic transport property is susceptible to the atomic crystal structure of two-dimensional materials. The combined electrical results above confirm that the inorganic selenium molecular mediator greatly maintains the atomic structure stability of sensitive materials during the fabrication of electronic devices, which profoundly improves the intrinsic carrier conductivity in electronic devices. The great electronic transport property and high-consistent electrical signals demonstrate that the inorganic selenium microlithography is highly compatible with the current industry CMOS (complementary metal oxide semiconductor) manufacturing processes for scalable integration.

## Discussion

We have developed an inorganic selenium-based microlithographic mediator for solvent-free processing of sensitive electronic materials. The selenium layer enables direct patterning through

---

localized photothermal sublimation under laser or plasma irradiation, eliminating chemical solvents or solutions and thereby streamlining conventional lithographic workflows. Furthermore, the weak interfacial adhesion between the selenium layer and substrate facilitates high-fidelity micropatterning and wafer-scale array fabrication with sharp edges and atomically flat surfaces via rapid physical peeling. Unlike conventional organic polymer composites, the single-element composition of the selenium mediator simplifies production, storage, and application. By utilizing inorganic molecular layers as protective barriers, this lithographic approach prevents solvent contact with sensitive materials while preserving their structural and electronic integrity. Experimental validation confirms that the solvent-free methodology enables non-destructive processing of delicate electronic components. Leveraging its compatibility with industrial standards, the process successfully fabricates monolayer MoS<sub>2</sub>-FET arrays with exceptional electronic homogeneity and on-off ratios exceeding 10<sup>8</sup>. This versatile microlithography strategy holds significant potential for advancing the microfabrication of emerging electronic materials and devices.

## Methods

**Inorganic selenium molecular microlithography process.** (1) Selenium molecule deposition. Selenium molecules were deposited on the substrate via thermal evaporation under vacuum conditions (1-5 Pa). The sublimation process was initiated at 150-200°C with a sample plate rotation speed of 50-100 rpm, enabling uniform film formation. (2) Laser/plasma exposure. The laser was directly exposed on the selenium film to form patterns. 532 nm and 633 nm laser beams were focused on the surface of the selenium film through an objective lens. The exposed local area of the selenium film can be precisely controlled by tuning the laser beam intensity, scanning speed, and scanning position. (3) Object material deposition. Functional halide layer ( $\text{PbBr}_2$ ,  $\text{PbI}_2$ ) and metal layers (Au, Sn, Cu) were deposited on patterned selenium films using magnetron sputtering or electron-beam evaporation. To enhance interfacial adhesion, a 5 nm Cr or Bi interlayer was introduced prior to Au deposition. (4) Selenium layer removal. Two solvent-free methods were employed. Mechanical peeling: A polydimethylsiloxane (PDMS) stamp was conformally attached to the selenium film (bubble-free interface verified by optical microscopy) and mechanically peeled in seconds, simultaneously removing excess selenium and overlying object layers. Thermal evaporation: Residual selenium was sublimated through vacuum annealing at 150 °C for 3 h, preserving substrate-bound patterns with atomic-level edge definition.

**Standard resist photolithography.** Standard photolithography used resist (AZ5214) and tetramethylammonium hydroxide (TMAH, 2.38%) developer (ZX-238). The resist was spin-coated on the silicon substrate and heated at 95 °C for 90 seconds. After light focusing and irradiation, resist then dissolved in developer and exposed to the designed window patterns.

**Materials synthesis.** Halide  $\text{PbBr}_2$  crystal flakes were obtained by chemical vapor deposition (CVD) growth in a one-inch horizontal quartz tube furnace under ambient pressure<sup>49</sup>. Atomic vapor was gradually deposited on fresh-cleaved mica substrates.

Alkali metal compound  $\text{LiInP}_2\text{S}_6$  single crystals were prepared by the chemical vapor transport (CVT) process<sup>50</sup>. First, raw  $\text{LiInP}_2\text{S}_6$  powder and  $\text{I}_2$  transporting agent were sealed in a quartz tube. The tube was placed in a two-zone furnace and heated to 660 °C (source zone) and 560 °C (sink zone) held for one week, and then cooled to ambient temperature. The  $\text{LiInP}_2\text{S}_6$  crystals were obtained on the sink side and mechanically exfoliated by tape to crystal nanoflakes. The exfoliated crystal flakes were transferred to the substrate for photolithography.

Organic-inorganic hybrid perovskite  $(\text{MP})_2\text{PbI}_4$  single crystals were prepared by solution cooling crystallization. Under stirring, 1 mmol of lead oxide (0.223 g) was first dissolved in a mixture of 3.5 mL of hydroiodic acid and 1.5 mL of hypophosphate solution, and then 1 mmol (155  $\mu\text{L}$ ) of MeOPEA was added to the solution. After stirring at 65 °C for 30 min, the solution was slowly cooled to room temperature at a cooling rate of 1 °C  $\text{h}^{-1}$ . Finally, orange perovskite  $(\text{MP})_2\text{PbI}_4$  crystals were obtained and then mechanically exfoliated by tape. The exfoliated crystal flakes were transferred to a silicon substrate for photolithography.

Phosphorus sulfide  $\text{MgPS}_3$  was synthesized by chemical vapor transport. Use Mg pellets, red phosphorus, and sulfur powder as raw materials. A total of 2 g of the raw materials was weighed according to the stoichiometric ratio. The mixed powder was loaded into a quartz tube, which was then evacuated to a vacuum of  $10^{-2}$  Pa and sealed. The sealed tube was placed in a dual-zone muffle furnace and subjected to the following program: heating to  $650$  °C (source zone) and  $500$  °C (deposition zone) over 20 hours, maintaining for 100 hours, cooling to  $250$  °C, and finally cooling naturally to room temperature. Colorless transparent sheet-like crystals were obtained from the quartz tube.

Black phosphorus crystals were purchased from Nanjing MKNANO Tech. Co., Ltd. Black phosphorus flakes were obtained by mechanically exfoliating the black phosphorus crystals.

**Materials characterizations.** The morphology images of Se film and patterns were obtained by an optical microscope (Olympus BX51). The thickness and roughness were determined by an atomic force microscope (AFM, Bruker Dimension Icon). The X-ray diffraction (XRD) patterns were collected with a Bruker D8 Advance by Cu-K $\alpha$  radiation at  $30$  kV and  $10$  mA with a scan step width of  $0.02$ °. Scanning electron microscope (SEM, FEI Quanta 650) was used to identify the morphology and elements. Raman spectrum and mapping (WITec Alpha300 Raman) were performed on a confocal microscope spectrometer with  $\times 100$  microscope objective. All Raman spectra were calibrated as a reference of silicon characteristic peak  $520$  cm $^{-1}$ .

**Film adhesion forces.** The film adhesion force was investigated on the scratching module of a nanomechanical testing system (Agilent Nano Indenter, G200). Interfacial adhesions between three films and silicon substrate were measured. Standard output load gradually increased from  $0$  mN to  $30$  mN with a scratching distance of about  $300$   $\mu\text{m}$ .

**Electronic device fabrication and measurement.** Mechanically exfoliated 2D materials were transferred on a cleaned  $\text{SiO}_2/\text{Si}$  substrate.  $\text{SiO}_2$  and Si were used as the back-gate insulator and electrode, respectively. For electronic device fabrication, metal Au layers as drain and source electrodes were performed to pattern by the selenium microlithography process. When the material on the substrate has a strong binding force with the selenium layer, the selenium film is removed by heating evaporation at  $200$  °C before PDMS mechanical stripping. The electronic current-voltage measurements were performed using a semiconductor device analyzer (Agilent B1500A) in a probe station (Lake Shore CRX-6.5K) at room temperature ( $\sim 300$  K).

## Data availability

Relevant data supporting the key findings of this study are available within the article and the Supplementary Information. All raw data generated during the study are available from the corresponding authors upon request.

## References

1. Orji N. G. et al. Metrology for the next generation of semiconductor devices. *Nat. Electron.* **1**, 532-547 (2018).
2. Wang Y. et al. Direct optical lithography of functional inorganic nanomaterials. *Science* **357**, 385-388 (2017).
3. Chen J. et al. Optoelectronic graded neurons for bioinspired in-sensor motion perception. *Nat. Nanotechnol.* **18**, 882-888 (2023).
4. Tao L. et al. Silicene field-effect transistors operating at room temperature. *Nat. Nanotechnol.* **10**, 227-231 (2015).
5. Meng W. et al. Three-dimensional monolithic micro-LED display driven by atomically thin transistor matrix. *Nat. Nanotechnol.* **16**, 1231-1236 (2021).
6. Zhong D. et al. High-speed and large-scale intrinsically stretchable integrated circuits. *Nature* **627**, 313-320 (2024).
7. Zheng Y.-Q. et al. Monolithic optical microlithography of high-density elastic circuits. *Science* **373**, 88-94 (2021).
8. Ito T., Okazaki S. Pushing the limits of lithography. *Nature* **406**, 1027-1031 (2000).
9. Tu M. et al. Direct X-ray and electron-beam lithography of halogenated zeolitic imidazolate frameworks. *Nat. Mater.* **20**, 93-99 (2021).
10. Luo C. et al. Review of recent advances in inorganic photoresists. *RSC Adv.* **10**, 8385-8395 (2020).
11. Jin F. et al.  $\lambda/30$  inorganic features achieved by multi-photon 3D lithography. *Nat. Commun.* **13**, 1357 (2022).
12. Liu T. et al. Ultrahigh-printing-speed photoresists for additive manufacturing. *Nat. Nanotechnol.* **19**, 51-57 (2023).
13. Sun K. et al. Three-dimensional direct lithography of stable perovskite nanocrystals in glass. *Science* **375**, 307-310 (2022).
14. Martínez E. D. et al. Recent advances on nanocomposite resists with design functionality for lithographic microfabrication. *Front. Mater.* **8**, 629792 (2021).
15. Li S.-L. et al. Charge transport and mobility engineering in two-dimensional transition metal chalcogenide semiconductors. *Chem. Soc. Rev.* **45**, 118-151 (2016).
16. Wei Z. et al. Scratching lithography for wafer-scale MoS<sub>2</sub> monolayers. *2D Mater.* **7**, 045028 (2020).
17. Kwon G. et al. Interaction- and defect-free van der Waals contacts between metals and two-dimensional semiconductors. *Nat. Electron.* **5**, 241-247 (2022).
18. Han J. W. et al. Recent patterning methods for halide perovskite nanoparticles. *Adv. Opt. Mater.*, 2200534 (2022).
19. Li Y. et al. Unravelling degradation mechanisms and atomic structure of organic-inorganic halide perovskites by Cryo-EM. *Joule* **3**, 2854-2866 (2019).
20. Shi E. et al. Two-dimensional halide perovskite lateral epitaxial heterostructures. *Nature* **580**, 614-620 (2020).
21. Yao Y. et al. Direct photolithography on molecular crystals for high performance organic optoelectronic devices. *J. Am. Chem. Soc.* **140**, 6984-6990 (2018).
22. Hong Y. et al. Solvent-free nanofabrication based on ice-assisted electron-beam lithography. *Nano lett.* **20**, 8841-8846 (2020).
23. Zhu L. et al. Scalable and versatile transfer of sensitive two-dimensional materials. *Nano lett.* **22**, 2342-2349 (2022).
24. Wang N. et al. Improving harsh environmental stability of few - layer black phosphorus by local charge transfer. *Adv. Funct. Mater.* **32**, 2203967 (2022).
25. Cheng H. C. et al. van der waals heterojunction devices based on organohalide perovskites and two-dimensional materials. *Nano lett.* **16**, 367-373 (2016).
26. Wang Y. et al. Ultraflat single-crystal hexagonal boron nitride for wafer-scale integration of a 2D-compatible high- $\kappa$  metal gate. *Nat. Mater.* **23**, 1495-1501 (2024).
27. Yannopoulos S. N. Structure and photo-induced effects in elemental chalcogens: a review on Raman scattering. *J. Mater. Sci. Mater. Electron.* **31**, 7565-7595 (2020).
28. Goldan A. H. et al. Molecular structure of vapor-deposited amorphous selenium. *J. Appl. Phys.* **120**, 135101 (2016).
29. Lu W. et al. Structure of amorphous selenium: small ring, big controversy. *J. Am. Chem. Soc.* **146**, 6345-6351 (2024).
30. Borchers T. H. et al. Cold photo-carving of halogen-bonded co-crystals of a dye and a volatile co-former using visible light. *Nat. Chem.* **14**, 574-581 (2022).
31. Meitl M. A. et al. Transfer printing by kinetic control of adhesion to an elastomeric stamp. *Nat. Mater.* **5**, 33-38 (2006).
32. Hsia K. J. et al. Collapse of stamps for soft lithography due to interfacial adhesion. *Appl. Phys. Lett.* **86**, 154106 (2005).
33. Liu L. et al. Scalable van der Waals encapsulation by inorganic molecular crystals. *Adv. Mater.* **34**, 2106041 (2022).
34. Chen C. et al. Growth of single-crystal black phosphorus and its alloy films through sustained feedstock release. *Nat. Mater.* **22**, 717-724 (2023).
35. Xia Y. et al. 12-inch growth of uniform MoS<sub>2</sub> monolayer for integrated circuit manufacture. *Nat. Mater.* **22**, 1324-1331 (2023).
36. Li T. et al. Epitaxial growth of wafer-scale molybdenum disulfide semiconductor single crystals on sapphire. *Nat. Nanotechnol.* **16**, 1201-1207 (2021).
37. Tao Q. et al. High-density vertical sidewall MoS<sub>2</sub> transistors through T-shape vertical lamination. *Nat. Commun.* **15**, 5774 (2024).
38. Sun L. et al. Concurrent synthesis of high - performance monolayer transition metal disulfides. *Adv. Funct. Mater.* **27**, 1605896 (2017).
39. Xie L. et al. Graphene-contacted ultrashort channel monolayer MoS<sub>2</sub> transistors. *Adv. Mater.* **29**, 1702522 (2017).

40. Yu H. et al. Eight In. Wafer-Scale Epitaxial Monolayer MoS<sub>2</sub>. *Adv. Mater.* **36**, 2402855 (2024).

41. Xie L. et al. A facile and efficient dry transfer technique for two-dimensional Van der Waals heterostructure. *Chin. Phys. B* **26**, 087306 (2017).

42. Wang Y. et al. Van der Waals contacts between three-dimensional metals and two-dimensional semiconductors. *Nature* **568**, 70-74 (2019).

43. Yang P. et al. Batch production of 6-inch uniform monolayer molybdenum disulfide catalyzed by sodium in glass. *Nat. Commun.* **9**, 979 (2018).

44. Liu L. et al. A mass transfer technology for high-density two-dimensional device integration. *Nat. Electron.* **8**, 135-146 (2025).

45. Nakatani M. et al. Ready-to-transfer two-dimensional materials using tunable adhesive force tapes. *Nat. Electron.* **7**, 119-130 (2024).

46. Li Z. et al. Residue-free wafer-scale direct imprinting of two-dimensional materials. *Nat. Electron.* **8**, 571-577 (2025).

47. Kalkan S. B. et al. High-performance monolayer MoS<sub>2</sub> field-effect transistors on cyclic olefin copolymer-passivated SiO<sub>2</sub> gate dielectric. *Adv. Opt. Mater.* **11**, 2201653 (2022).

48. Sun H. et al. Hole-doping-assisted epitaxial growth of wafer-scale rhombohedral-stacked bilayer transition-metal dichalcogenides single crystals. *Nat. Commun.* **16**, 9820 (2025).

49. He X. et al. Universal vapor-phase synthesis of large-scale ultrathin perovskites with superior stability for photodetectors and image sensors. *Adv. Funct. Mater.* **34**, 2313163 (2024).

50. Liang J. et al. Anomalous superionic conductivity in van der Waals lithium thiophosphates triggered by interlayer molecules. *Energy Environ. Sci.* **17**, 3210-3217 (2024).

## Acknowledgements

This study was supported by National Natural Science Foundation of China (92580121 [H. L.], 22535004 [C. Z., T. Z.], U22A20140 [H. L.], 22350003 [T. Z.], 22409068 [C. Z.]), National Key Research and Development Program of China (2023YFB2503903 [H. L.]), the Postdoctoral Fellowship Program of CPSF (GZC20230879 [C. Z.], YJB20250020 [C. Z.]), Project funded by China Postdoctoral Science Foundation (2023M741247 [C. Z.]). We acknowledge the technical support from Huazhong University of Science and Technology Analytical & Testing Center.

## Author contributions

H. L. and T. Z. supervised the research project. C. Z. performed the microlithography process, optical microscopy, Raman spectrum, X-ray diffraction pattern, and film adhesion force measurement. C. Z., Y. X., and Y. L. (Y. Liu) carried out the electronic device fabrication and measurement. X. W. and C. Z. conducted the atomic force microscopy measurement. G. D. conducted the scanning electron microscopy. C. Z., Y. X., J. L., S. W., X. Z., Y. L. (Y. Li), K. L., H. L., and T. Z. designed the experiment scheme. J. L., Z. S., X. H., and Y. M. synthesized the crystal materials. C. Z., K. L., H. L., and T. Z. prepared the manuscript.

## Competing interests

The authors declare no competing interests.

## Figure Legends/Captions

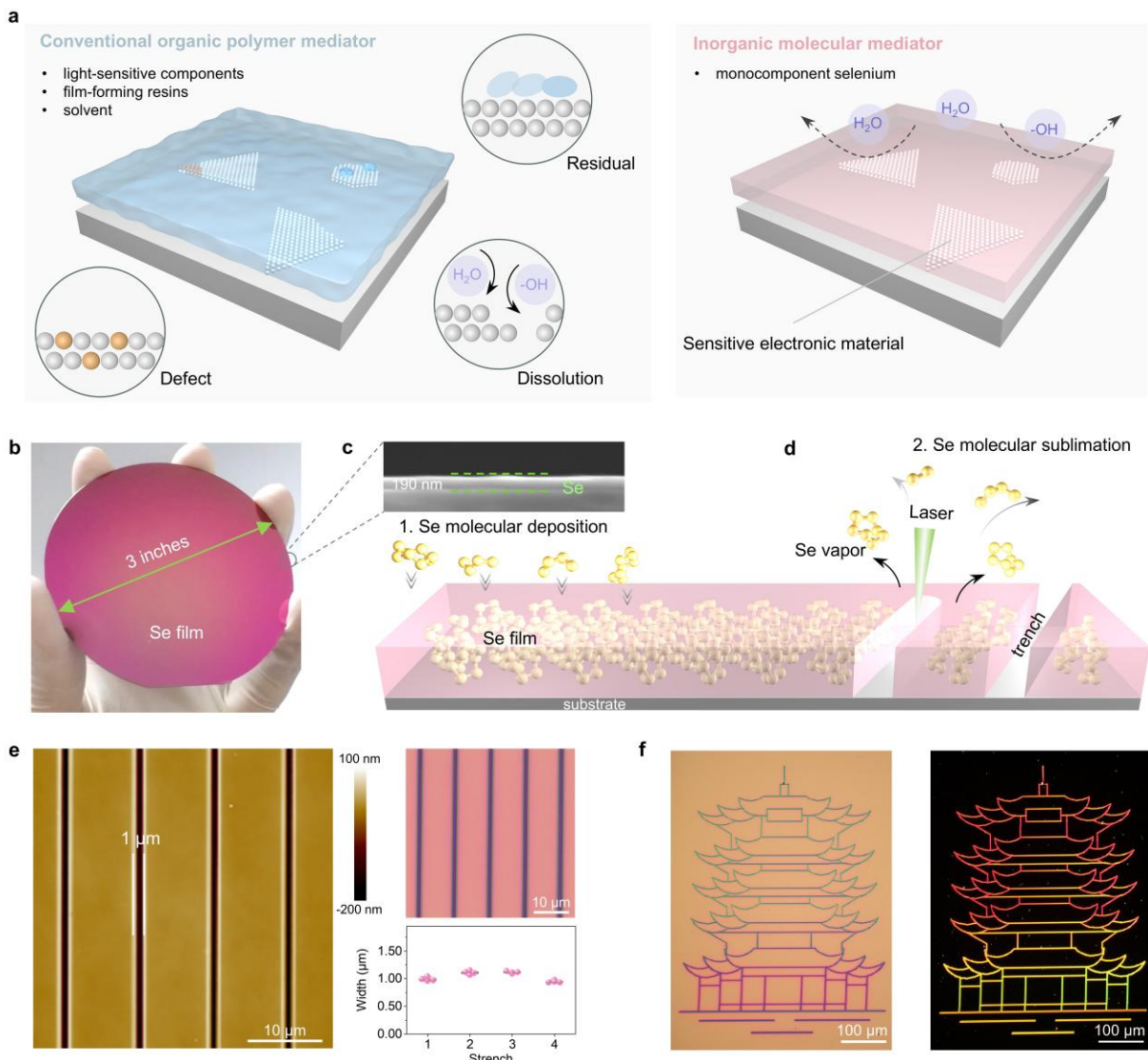


**Fig. 1 Inorganic selenium molecular microlithographic mediator.** **a**, Schematic of lithography using conventional inorganic polymer resist and organic selenium resist to sensitive electronic materials. **b**, Photograph of Se film deposited on Si wafer. **c**, Scanning electron microscopy (SEM) image of cross section of Se film deposited on Si substrate. **d**, Schematic illustration of Se molecular deposition and Se molecular photothermal sublimation. **e**, Atomic force microscope (AFM, left) and scanning electron microscopy (SEM, right) topographic images of the Se trench patterns, corresponding statistical analyses for four trench widths. **f**, Optical light field (left) and dark field (right) images of ancient Chinese architecture tower patterned on Se film surface by controlled laser direct writing.

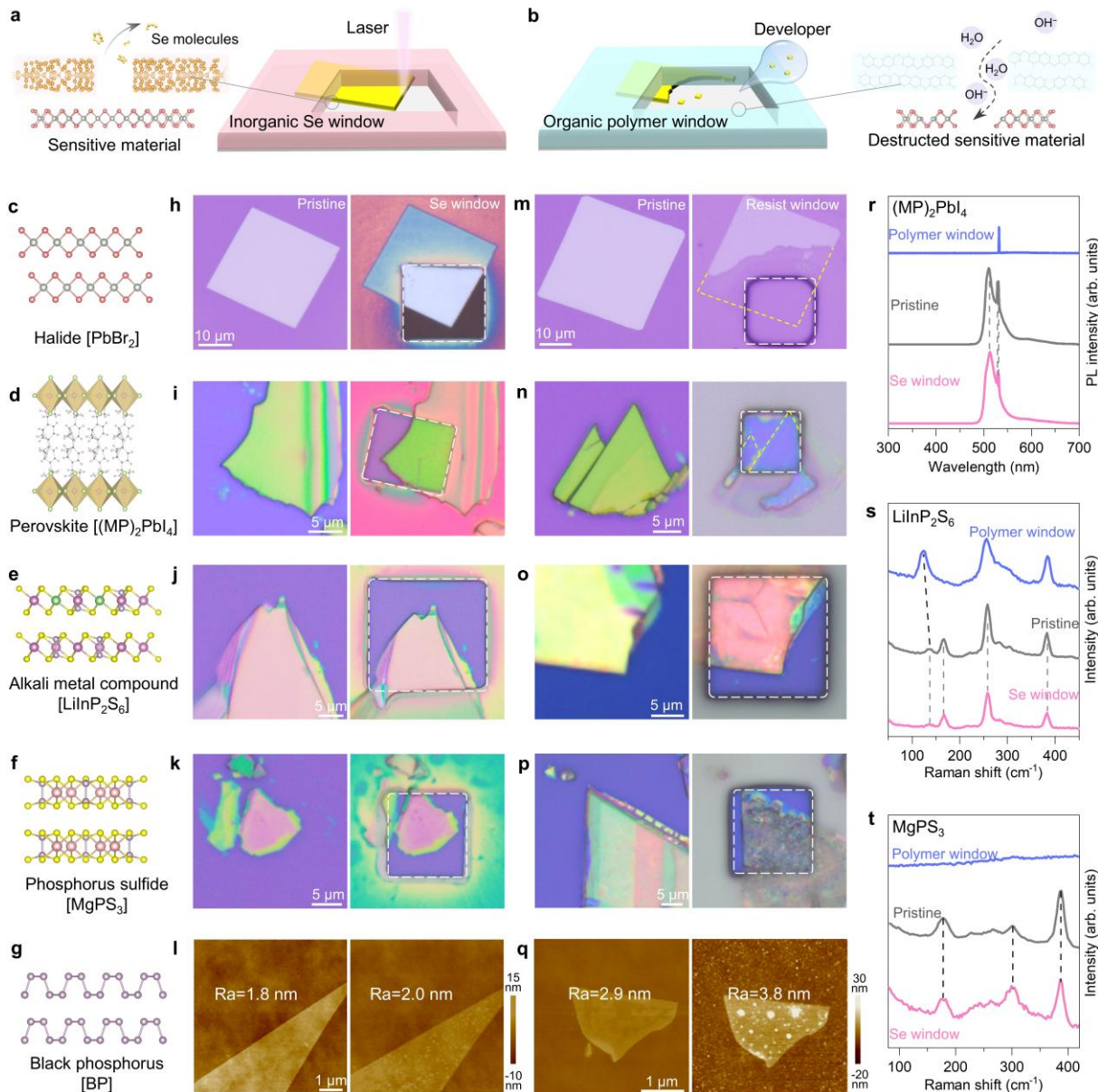


**Fig. 2 Comparison of sensitive materials possessing by inorganic selenium lithography and standard organic polymer lithography.** **a**, Schematic illustration of direct selenium lithography for sensitive material. **b**, Schematic illustration of standard resist lithography for sensitive material. **c-g**, Typical sensitive electronic materials, including halide  $[\text{PbBr}_2]$ , perovskite  $[(\text{MP})_2\text{PbI}_4]$ , alkali metal compound  $[\text{LiInP}_2\text{S}_6]$ , phosphorus sulfide  $[\text{MgPS}_3]$ , black phosphorus  $[\text{BP}]$ . **h-k**, Optical images of four sensitive materials before and after laser direct writing Se window. **l**, AFM images of black phosphorus before covering Se layer and after removing Se layer. Ra indicates the roughness. **m-p**, Optical images of four sensitive materials before and after developing polymer window. **q**, AFM images of black phosphorus before covering polymer layer

---

and after removing polymer layer. **r**, Photoluminescence (PL) spectroscopy lines of perovskite  $[(\text{MP})_2\text{PbI}_4]$  in pristine materials, Se window, and polymer window. **s,t**, Raman lines of  $\text{LiInP}_2\text{S}_6$  and  $\text{MgPS}_3$  in pristine materials, Se window, and polymer window.

ARTICLE IN PRESS

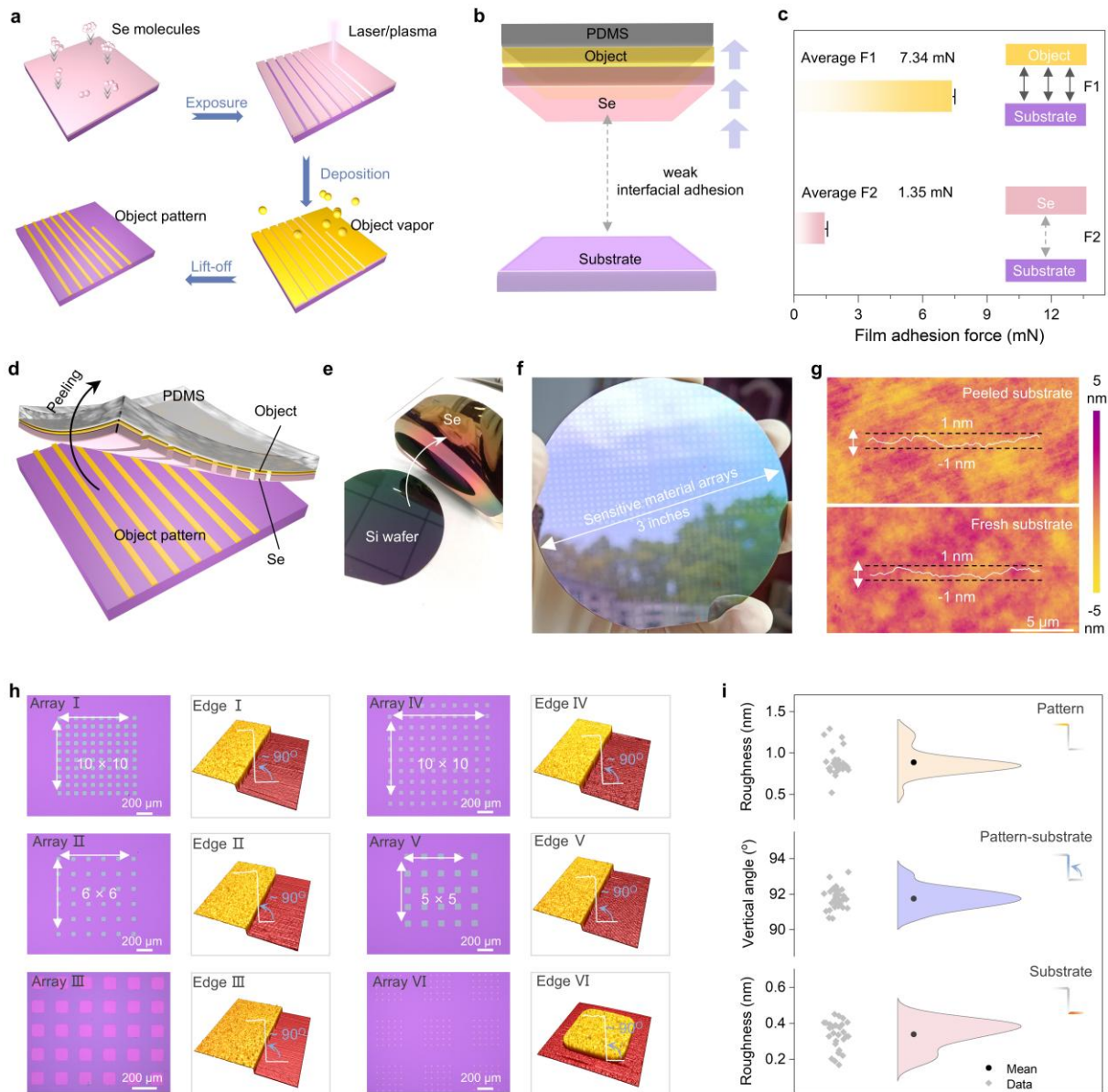


**Fig. 3 Wafer-scale micropatterns by physical lift-off process of selenium layer.** **a**, Schematic of solvent-free selenium microlithography process, including selenium molecular deposition, laser/plasma exposure, object material deposition, and selenium molecular removal. **b**, Force analysis of interfacial adhesion between the contact films under polydimethylsiloxane (PDMS) layer. **c**, Adhesion force measurement between the object layer and the substrate (F1), the Se layer and the substrate (F2). The measured object material is a metal Au layer. The error bars show the standard deviation of the mean in three adhesion values. **d**, Schematic illustration of selenium lithography for patterning by physical peeling process. **e**, PDMS assisted peeling process of Se layer away from Si wafer substrate. **f**, Photograph of the solvent-sensitive

material wafer ( $\text{PbBr}_2$  arrays, 3 inches) after physical peeling. The reflection in the wafer is cloud, sky, tree, and building in campus. **g**, AFM images of peeled and fresh  $\text{SiO}_2/\text{Si}$  substrate surface. White line profiles are surface height curves. **h**, Optical images of the pattern arrays in six regions, and three-dimensional AFM images of the pattern edge topography in the six arrays. The angle is between the substrate and the vertical edge of the pattern. **i**, Half violins of pattern roughness, pattern-substrate vertical angle, and substrate roughness from 30 pattern locations.

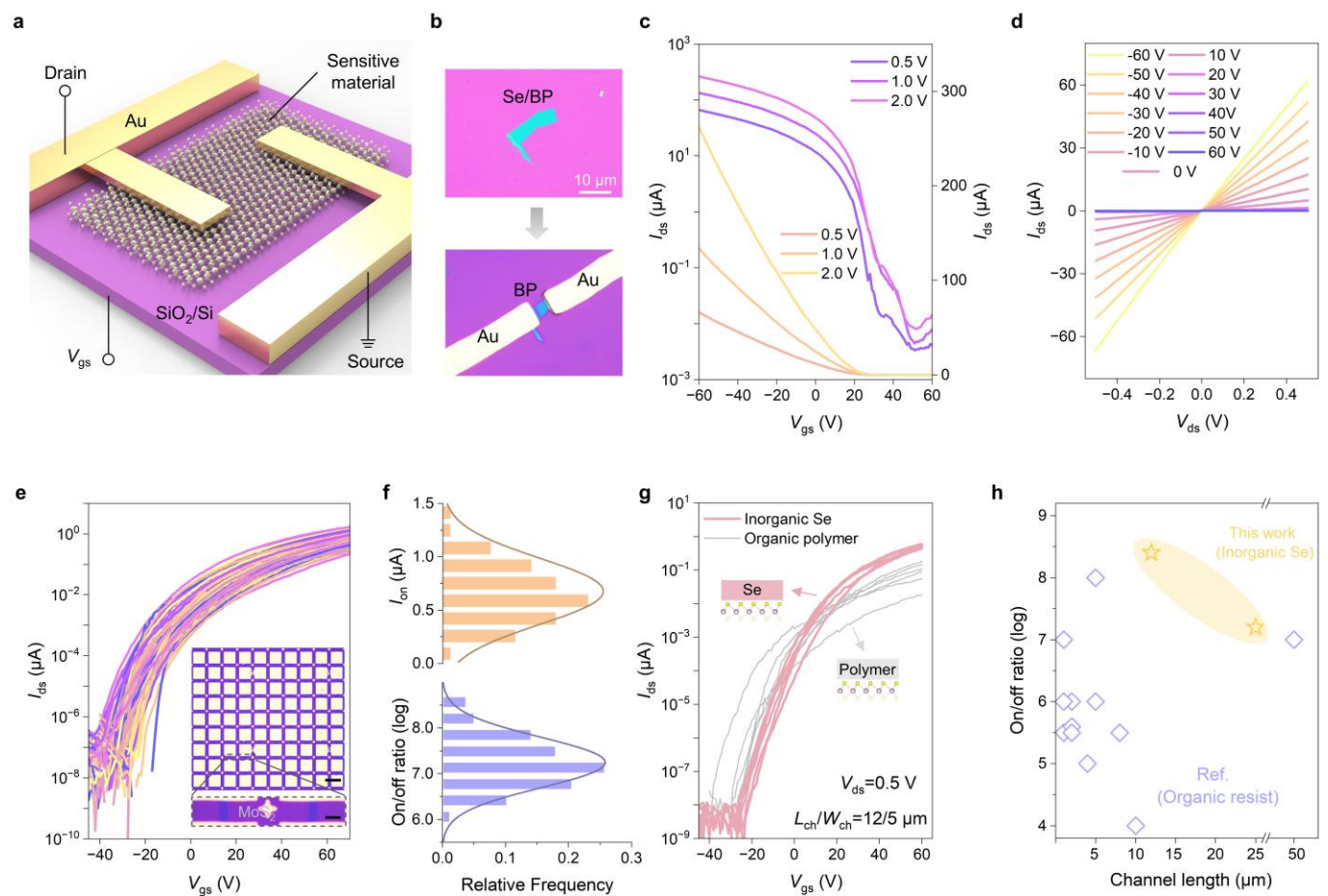


**Fig. 4 Field effect transistor device by Se-assisted microlithography.** **a**, Schematic of back-gated black phosphorus (BP) electronic device using  $\text{SiO}_2$  (300 nm) layer as gate dielectric, Si layer as back gate, metal as drain and source. **b**, Optical images of few-layer BP flake covered by Se molecular layer and single BP device. **c**, Transfer characteristic curves of BP field effect transistor under drain-source voltages at 0.5 V, 1.0 V, and 2.0 V. **d**, Output characteristic curves of BP field effect transistor under gate voltages from -60 V to 60 V with 10 V steps.  $V_{gs}$ , gate-source voltage;  $I_{ds}$ , drain-source current;  $V_{ds}$ , drain-source voltage. **e**, **f**, On/off ratio distribution. **g**, Transfer characteristic curves of BP field effect transistor under drain-source voltages at 0.5 V. The inset shows AFM images of the substrate surface. **h**, On/off ratio vs. channel length. **i**, Violin plots of pattern roughness, pattern-substrate vertical angle, and substrate roughness.

Transfer characteristics of monolayer MoS<sub>2</sub> field effect transistors (FET) driven drain-source voltage at 0.5 V. Insert: optical image of 80 FET arrays fabricated by the Se-assisted microlithography. Scale bar, 100  $\mu$ m. Channel length and width,  $L_{ch}/W_{ch}=25/10$   $\mu$ m. Zoomed-in image: scale bar, 20  $\mu$ m. **f**, Corresponding histogram statistical analyses for on-current  $I_{on}$  and on/off ratio with normal distribution curves. **g**, Comparison of transfer characteristics of MoS<sub>2</sub> array transistors fabricated with inorganic Se layer (red lines) and organic polymer layer (grey lines),  $L_{ch}/W_{ch}=12/5$   $\mu$ m. **h**, Comparison of the average on/off ratio of back-gated MoS<sub>2</sub> FETs with SiO<sub>2</sub> dielectric fabricated by the inorganic Se microlithography and the reported organic resist lithography<sup>17,37-48</sup>.

**Editorial Summary**

Conventional organic polymeric resists and chemical solutions used in microlithographic techniques can damage sensitive materials. Here, the authors report the application of inorganic selenium molecules as a lithographic mediator and encapsulation layer during the processing of various sensitive materials, such as perovskites and black phosphorus.

**Peer review information:** *Nature Communications* thanks Peng Chen, Zhiwei Li, and the other, anonymous, reviewer for their contribution to the peer review of this work. A peer review file is available.